ACS OMEGA

Article

http://pubs.acs.org/journal/acsodf

Core–Shell Structured Polyamide 66 Nanofibers with Enhanced Flame Retardancy

Linhong Xiao,[†,#] Linli Xu,[†,#] Yuying Yang,[‡] Sheng Zhang,[‡] Yong Huang,[†] Christopher W. Bielawski,[§,∥,⊥] and Jianxin Geng*[,†]

[†]Technical Institute of Physics and Chemistry, Chinese Academy of Sciences, 29 Zhongguancun East Road, Haidian District, Beijing 100190, China

[‡]Key Laboratory of Carbon Fiber and Functional Polymers, Beijing University of Chemical Technology, 15 North Third Ring Road, Chaoyang District, Beijing 100029, China

[§]Center for Multidimensional Carbon Materials (CMCM), [∥]Department of Chemistry, Ulsan National Institute of Science and Technology (UNIST), and [⊥]Department of Energy Engineering, Ulsan National Institute of Science and Technology (UNIST), Ulsan National Institute of Science and Technology (UNIST), 50 UNIST-gil, Ulsan 44919, Republic of Korea

S *Supporting Information*

ABSTRACT: We report the preparation of polymer nanofibers with enhanced flame retardancy by coaxial electrospinning polyamide 66 (PA 66) and nanoscale graphene hybridized with red phosphorus (NG–RP). Transmission electron microscopy and energy-dispersive X-ray spectroscopy revealed that the nanofibers contained a NG–RP-based core surrounded by a PA 66 shell. The flame-retardant characteristics of the nanofibers were investigated by thermal gravimetric analysis, micro combustion calorimetry, and a series of vertical flame tests. The encapsulation of the NG–RP not only enhanced the flame-retardant characteristics of the nanofibers, but also improved their mechanical properties while maintaining the color and luster of the polymer, making the resultant nanofibers appropriate for use in a wide range of applications.

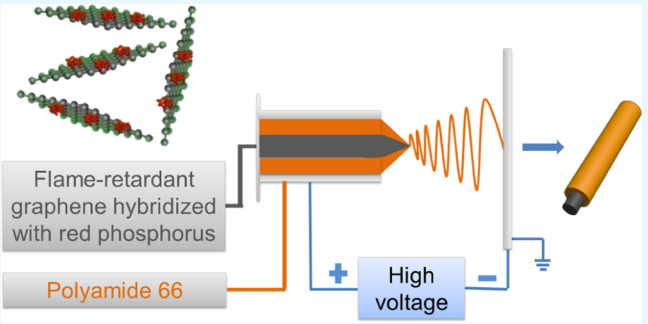

INTRODUCTION

The electrospinning of synthetic polymers continues to grow in popularity as a method because it not only enables fine control over the architecture[1−3] and dimensions of the resultant nanofibers,[4] but it can also be conveniently scaled.[5] As a result, electrospun nanofibers have been extensively used in a variety of applications, including drug delivery,[6] tissue engineering,[7] and energy harvesting.[8] Unfortunately, neat polymer nanofibers are often combustible and,[9] as a result, there is currently a need for flame-retardant derivatives. Although the use of polymers with noncombustible functional groups[10] and surface modification strategies represent established approaches for enhancing the flame retardancies of polymer nanofibers,[11−13] the former often suffers from technical complexity and the latter diminishes fiber durability and esthetics (i.e., color options and luster). As a result, the development of new methods for preparing flame-retardant polymer nanofibers is warranted.

Coaxial electrospinning typically produces nanofibers with a polymeric material as the shell and a functional component as the core. As the two structural components are often synergistic,[14,15] we hypothesized that nanofibers containing flame-retardant cores should reduce the combustibility of the polymeric shells. Therefore, a primary aim of our efforts was to produce core–shell structured polymer nanofibers via coaxial electrospinning.

Graphene has recently attracted significant attention for use in flame-retardant polymer-based composites,[16,17] in part because it forms a protective char layer upon combustion[18] and can be hybridized with other flame retardants.[16,19] Despite these advantages, several challenges have prevented graphene from being broadly used in applications that require a resistance to combustion. First, it is often difficult to evenly distribute graphene in synthetic polymer matrices, which can compromise the mechanical properties of the resulting composites.[20] Second, the flame-retardant efficiency of graphene is relatively low and thus combination with other types of flame retardants is usually required.[21,22] Finally, the synthesis of graphene-based flame retardants requires the use of hazardous and toxic chemicals, which inherently restricts utility and scalability.[16] To overcome the aforementioned drawbacks, we recently reported a one-step ball-milling method for hybridizing red phosphorus

Received: April 4, 2017
Accepted: June 2, 2017
Published: June 15, 2017

DOI: 10.1021/acsomega.7b00397
ACS Omega 2017, 2, 2665−2671

(RP) with graphene.[23] The resultant composite was found to significantly improve the flame retardancy as well as the mechanical properties of polymer foams.

Building on our previous work, we report the first flame-retardant nanofibers that feature flame-retardant cores and polymer shells. The nanofibers were fabricated by the coaxial electrospinning of polyamide 66 (PA 66) with a composite of nanoscale graphite (NG) and RP. PA 66 was selected as the polymer component due to its excellent mechanical properties, good processability, and broad utility.[24,25] NG was chosen as a source of graphene because it was found to increase the dispersibility of the RP particles on the surface of the graphene platelets, which synergistically enhanced the flame retardancy of the resultant nanoscale graphene hybridized with RP (NG−RP) nanoplatelets. Compared to the neat nanofibers of PA 66, those that contained NG−RP exhibited enhanced flame-retardant and mechanical properties, while maintaining the color and luster intrinsic to PA 66.

RESULTS AND DISCUSSION

Preparation and Characterization of the NG−RP Nanoplatelets. The NG−RP nanoplatelets were prepared in one-step by ball milling NG with RP. NG was used as the starting material because it improved the dispersibility of RP and facilitated access to the platelets of graphene (see Figure S1). As shown in Figure 1, the morphologies and sizes of NG, RP, and the NG−RP nanoplatelets were characterized by electron microscopy. Scanning electron microscopy (SEM) revealed that the dimensions of the NG and RP particles were on the order of ca. hundreds of nanometers and ca. micrometers, respectively. In contrast, the dimensions of the NG−RP nanoplatelets were found to be significantly smaller, presumably due to the shear forces generated during ball milling. The reduction in particle size was subsequently confirmed by transmission electron microscopy (TEM). In addition, energy-dispersive X-ray spectroscopy (EDS) indicated that elemental carbon, oxygen, and phosphorus were homogeneously distributed in the NG−RP composites (see Figure S2).

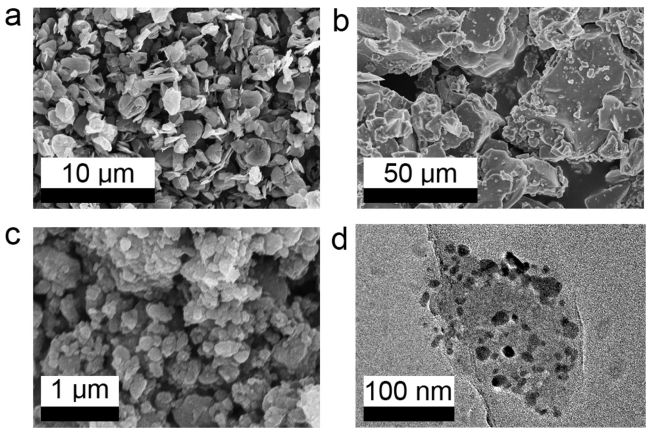

Figure 1. Summary of morphological characterization data. SEM images of (a) NG, (b) RP, and (c) the NG−RP platelets. (d) A TEM image of a NG−RP platelet.

The structure displayed by the NG−RP nanoplatelets was also investigated by X-ray diffraction (XRD) analysis. As shown in Figure 2a, the XRD pattern recorded for NG exhibited a strong and sharp (002) diffraction peak at 26.5°, which corresponded to an interlayer *d*-spacing of 0.34 nm. Consistent with the exfoliation of NG during the ball-milling process, the XRD pattern recorded for NG−RP composite did not exhibit a signal at the aforementioned angle. X-ray photoelectron spectroscopy (XPS) measurements were performed to gain a deeper insight into the chemical composition of the aforementioned materials. As shown in Figure 2b, NG exhibited a strong C 1s signal at 285 eV, along with a weak O 1s signal at 533 eV. For comparison, the NG−RP nanoplatelets exhibited increased O 1s and C 1s signals, as well as two new signals at 192 and 134 eV, which were assigned to the P 2s and P 2p orbitals, respectively. The increased intensity of the O 1s signal may be attributed to inadvertent oxidation that occurred when the as-prepared NG−RP composite was exposed to air after the ball-milling process.[16] Regardless, the detection of the P 2s and P 2p signals indicated that RP was hybridized with NG. Deconvolution of the high resolution C 1s XPS spectrum revealed that species containing C−C, C−P, and C−O bonds were present (Figure S3), which further supported the conclusions that hybridization as well as oxidation had occurred.[26,27] Additional structural elucidation was obtained by fitting the high resolution P 2p XPS spectrum recorded for NG−RP. The presence of P $2p_{3/2}$ and P $2p_{1/2}$ species at 130.2 and 131.0 eV was assigned to RP in the NG−RP nanoplatelets, and the P $2p_{3/2}$ and P $2p_{1/2}$ signals centered at 134.5 and 135.3 eV were consistent with the presence of phosphate.

As summarized in Figure 2c, Raman spectroscopy further supported the structural assignment. NG was minimally defective as the intensity ratio of the D:G bands (I_D/I_G) was measured to be ∼0.21. In contrast, I_D/I_G of NG−RP was determined to be 1.05, which is consistent with the presence of a significant number of structural defects, which may have occurred upon oxidation and/or exfoliation.[28] As will be discussed below, the aforementioned structural features play important roles in improving the flame-retardant and mechanical properties of the NG−RP-containing polymer nanofibers.[29]

To investigate the thermal stability of the NG−RP particles, a series of TGA measurements were independently performed under atmospheres of nitrogen or air. As shown in Figure 2d, the NG−RP particles exhibited three weight loss stages: (i) below 200 °C, due to evaporation of absorbed moisture; (ii) 200−500 °C, due to condensation of phosphonic acid;[17] and (iii) above 600 °C, due to pyrolysis of graphitic carbon and residual phosphorus. For comparison, the TGA data recorded for the NG−RP nanoplatelets under air exhibited a weight increase between 226−540 °C, presumably due to oxidation of RP (Figure S4). Significant weight loss occurred around 575 °C and was attributed to the condensation of phosphonic acid.

Preparation of the Core−Shell Structured Nanofibers. After investigating their morphology and composition, the NG−RP nanoplatelets were encapsulated by PA 66 and incorporated into nanofibers. To tune the content of NG−RP in the resultant nanofibers, polymer solutions with initial concentrations of 15, 17.5, or 20 wt % were independently used for the coaxial electrospinning process. The resulting fibers were labeled as NG−RP@PA 66 (1:7.5), NG−RP@PA 66 (1:8.75), and NG−RP@PA 66 (1:10), respectively; the ratios in parentheses refer to the weight ratios of NG−RP:PA 66 in the nanofiber feedstocks. As a control, neat PA 66 nanofibers were also prepared by electrospinning the polymer in the absence of the NG−RP platelets.

DOI: 10.1021/acsomega.7b00397
ACS Omega 2017, 2, 2665−2671

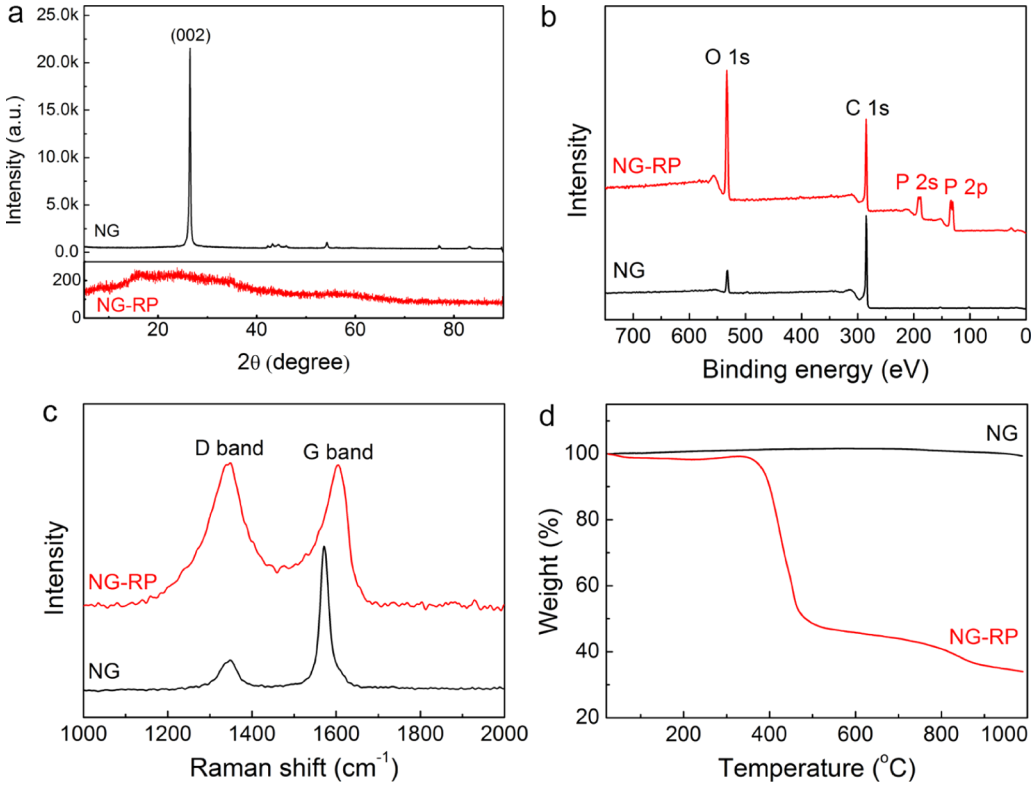

Figure 2. (a) XRD patterns, (b) XPS survey spectra, (c) Raman spectra, and (d) thermal data recorded for NG and the NG−RP nanoplatelets (indicated). The thermogravimetric analysis (TGA) data were collected under nitrogen.

SEM revealed that the nanofibers exhibited smooth surfaces and were randomly distributed on the underlying substrate (Figure 3a−c). The use of relatively concentrated solutions of PA 66 in the electrospinning process afforded nanofibers with larger average diameters (from 225 to 425 nm) (Figure 3d−f). Unlike the uniform contrast that was observed in the TEM images recorded for the neat PA 66 nanofibers (Figure S5), the images of those containing NG−RP exhibited dark and bright regions with complete concentricity (Figure 3g−i), which is consistent with a solid structure. The core−shell structures of the NG−RP@PA 66 nanofibers as well as the uniform dispersion of NG−RP in the cores were confirmed using TEM. Moreover, EDS elemental mapping indicated that phosphorus was uniformly dispersed along the NG−RP@PA 66 nanofibers (Figure S6).

To explore how the incorporation of the NG−RP nanoplatelets influenced the mechanical properties displayed by the corresponding nanofibers, a series of tensile tests were performed. As summarized in Figure 4, the tensile strength and Young's modulus of the fabrics prepared using neat PA 66 nanofibers were measured to be 6.2 and 69.0 MPa, respectively. Incorporating NG−RP into the cores of the nanofibers enhanced their mechanical properties. For example, a fabric containing the NG−RP@PA 66 (1:7.5) nanofibers exhibited a tensile strength of 9.3 MPa and a Young's modulus of 119.2 MPa. The enhanced mechanical properties of the NG−RP@PA 66 nanofibers were attributed to the incorporation of NG−RP nanoplatelets of high mechanical strength as well as their uniform dispersion along the cores of the nanofibers.

Evaluation of the Flame-Retardant Properties of the Core−Shell Structured Nanofibers. To ascertain how the NG−RP nanoplatelets influenced the thermal stabilities displayed by the NG−RP@PA 66 nanofibers, a series of TGA measurements were performed. The initial decomposition temperature at which a weight loss of 5% occurs has been used as an indicator of polymer thermal stability.[30−33] As shown in Figure 5, neat PA 66 nanofibers exhibited such decomposition at 314.2 °C, which was lower than that recorded for the NG−RP@PA 66 nanofibers (341.1−347.8 °C; see Table S1). In addition, the content of NG−RP in the corresponding nanofibers was estimated from the residual masses and found to be in agreement with the relative weight ratios of the PA 66 and NG−RP feedstocks.

The char residues formed after thermal degradation were also examined and appeared to correlate with the flame-retardant properties of the nanofibers. For example, neat PA 66 nanofibers afforded a char yield of ca. 0.41% at 700 °C, however the char yields given by the NG−RP@PA 66 nanofibers were significantly higher (up to 6.37% for the NG−RP@PA 66 (1:7.5) nanofibers at the same temperature). We surmised that NG−RP significantly improved the char formation properties of the PA 66 nanofibers by acting as a physical barrier and catalyzed the charring effect of phosphate.[34]

Because the NG−RP@PA 66 nanofibers exhibited relatively high thermal stabilities, we evaluated their flammability by subjecting nanofiber-derived fabrics to a flame for 12 s (ASTM D6413−11a). As a control, a fabric prepared using the neat PA 66 nanofibers was also tested. As shown in Figure 6, the NG−RP-containing fabrics required longer periods of time to ignite and less damage was observed when compared to that of the control. Indeed, all of the fabrics that contained NG−RP self-extinguished the propagating flame, which left the upper portions of the test samples unburned (Figures 6b−d). The aforementioned results demonstrate that the NG−RP nano-

DOI: 10.1021/acsomega.7b00397
ACS Omega 2017, 2, 2665−2671

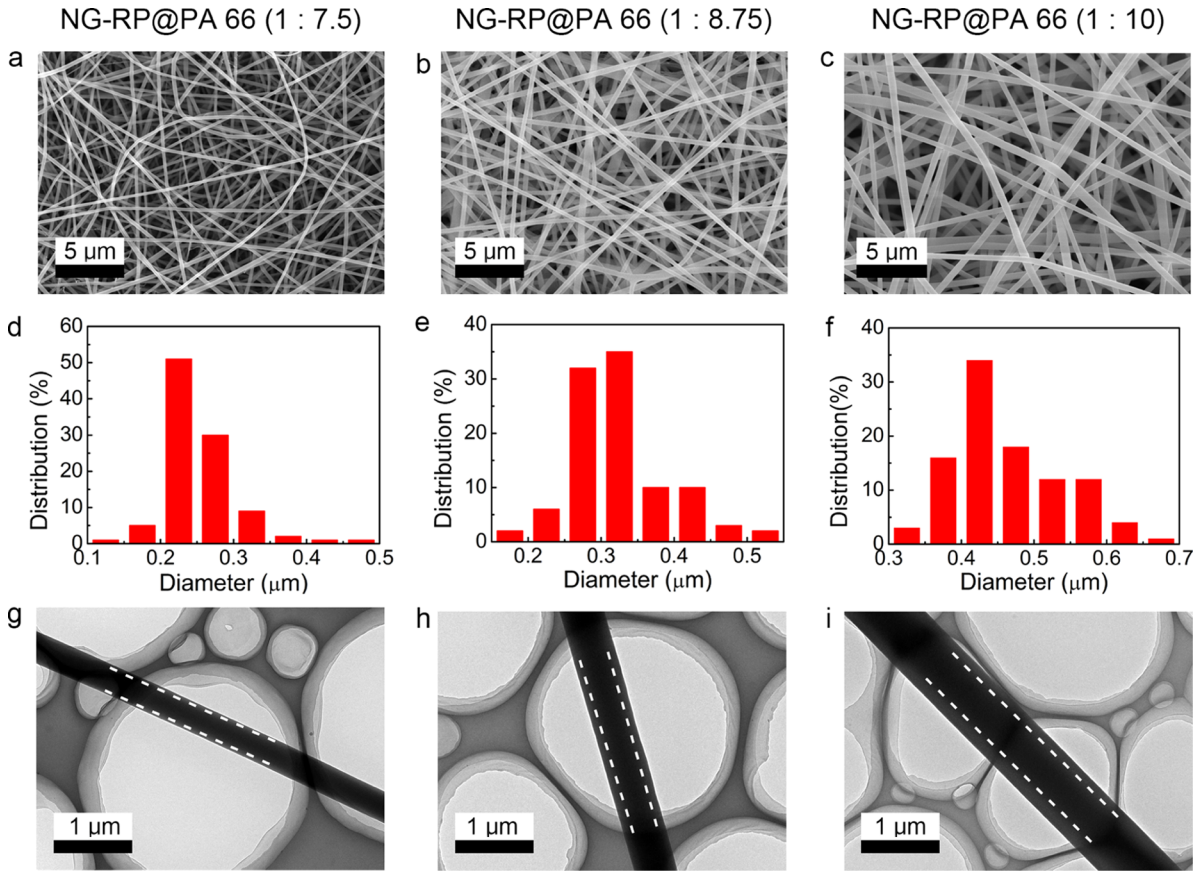

Figure 3. SEM images recorded of the (a) NG−RP@PA 66 (1:7.5), (b) NG−RP@PA 66 (1:8.75), and (c) NG−RP@PA 66 (1:10) nanofibers. The corresponding diameter distributions are shown in panels (d−f) and were obtained by counting 100 randomly chosen nanofibers. TEM images recorded of the (g) NG−RP@PA 66 (1:7.5), (h) NG−RP@PA 66 (1:8.75), and (i) NG−RP@PA 66 (1:10) nanofibers. The white dashed lines denote the boundaries between the core and the shell regions.

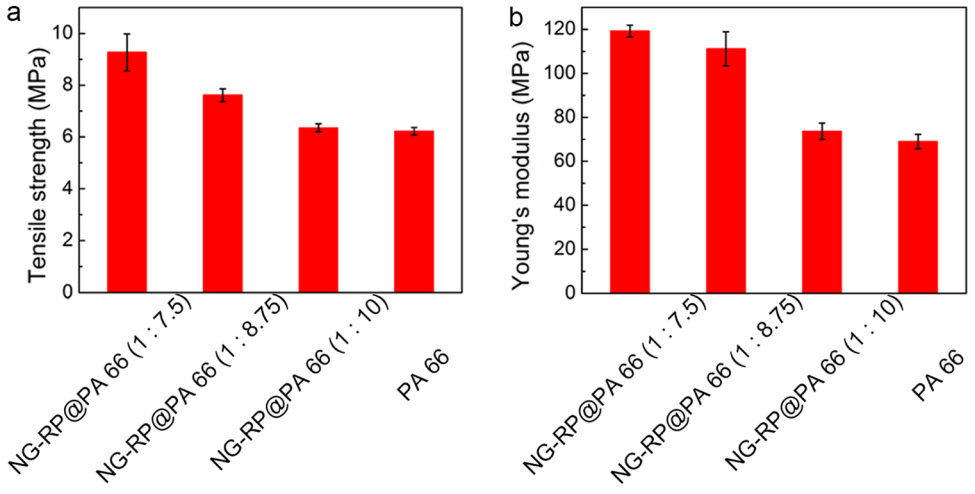

Figure 4. Selected mechanical properties measured for fabrics prepared using various nanofibers (indicated). (a) Tensile strength and (b) Young's modulus values. The error bars represent the standard deviations of data obtained from three separate experiments.

platelets effectively enhanced the flame retardancy of the PA 66 nanofibers.

The flame retardancy of the NG−RP@PA 66 nanofibers was further evaluated using micro combustion calorimetry (MCC) as this is an established technique for evaluating material combustion characteristics.[22,35] As summarized in Figure 7, heat release rates (HRR) were measured as a function of temperature for neat PA 66 as well as for the NG−RP-containing nanofibers. The total heat release (THR) value for the neat PA 66 nanofibers was measured to be 12.55 kJ g^{-1} with a peak HRR (pHRR) of 150.8 W g^{-1}. As summarized in Table S2, encapsulating NG−RP in the cores of the nanofibers sharply reduced the corresponding pHRR and THR values. For example, the NG−RP@PA 66 (1:7.5) nanofibers exhibited THR and pHRR values of 6.21 kJ g^{-1} and 110.3 W g^{-1}, respectively, which decreased by ca. 50.5 and 26.9%,

DOI: 10.1021/acsomega.7b00397
ACS Omega 2017, 2, 2665−2671

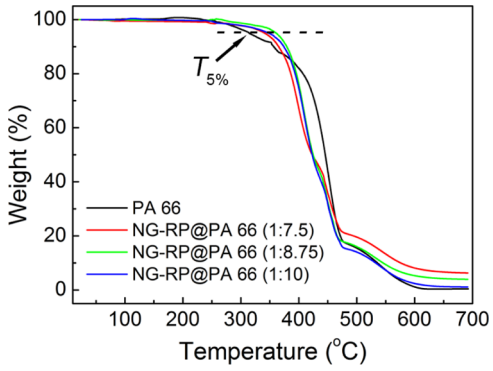

Figure 5. TGA curves of neat and NG−RP@PA 66 nanofibers obtained under an atmosphere of air.

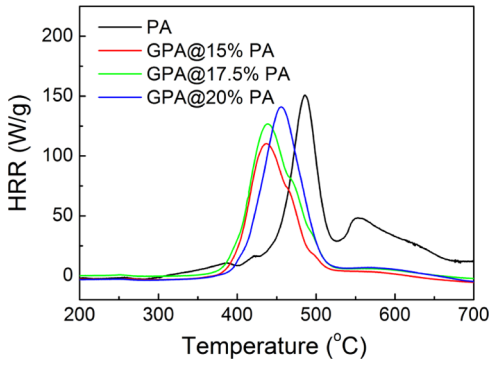

Figure 7. HRR vs temperature data recorded for various nanofibers (indicated).

respectively, when compared with the analogous values measured for the neat PA 66 nanofibers. The NG−RP-containing nanofibers were also found to display pHRR at temperatures lower than that of the neat PA 66 nanofibers, which may be due to the high thermal conductivity of the NG−RP particles. Regardless, the lower pHRR and THR values were attributed to the formation of high char residues during combustion, which decreased the release of gases and thus attenuated the HRR.[34]

CONCLUSIONS

In summary, core−shell structured PA 66 nanofibers with enhanced flame retardancy were prepared by encapsulating NG−RP platelets using a coaxial electrospinning method. The NG−RP platelets were prepared by ball milling NG and RP. The use of NG facilitated the formation of nanoscale graphene platelets, which further improved the dispersibility of the RP nanoparticles. Although the NG−RP@PA 66 nanofibers exhibited similar surface morphologies and sizes to those prepared using neat PA 66, the mechanical and flame-retardant properties of the former were considerably improved. The enhancements were attributed to the homogeneous distribution of and the flame retardancy intrinsic to the NG−RP nanoplatelets. In addition, the color and luster of PA 66 were maintained in the resulting nanofibers, which should facilitate their use in a wide range of applications. Considering that the coaxial electrospinning methodology described herein is straightforward to perform, inexpensive, and environmentally-benign, we expect that it will facilitate the realization of new classes of high performance, flame-retardant polymer nanofibers.

EXPERIMENTAL SECTION

Materials. PA 66 (Polynil P50 FI; Nilit America Co., Ltd.) was purified by dissolving the polymer in formic acid followed by pouring the resulting solution into excess methanol. A precipitate formed, which was subsequently collected and then dried in a vacuum oven set at 45 °C for 24 h. NG with an average diameter of 500 nm was obtained from Qingdao Tianheda Graphite Co., Ltd. RP (98.5%, analytical reagent) was purchased from Aladdin Industrial Co., Ltd. All other chemicals were purchased from Sinopharm Chemical Co., Ltd., and used as received.

Synthesis of NG−RP. A stainless steel capsule (100 mL) containing stainless steel balls (diameter: 5 mm, 250 g total) was charged with NG (2.5 g) and RP (5.0 g). The capsule was sealed under argon, affixed to a planetary ball mill machine, and agitated at 480 rpm for 48 h. The resultant products were carefully collected and then dried in a vacuum oven set at 45 °C for 12 h. CAUTION: the materials obtained using this method are prone to combustion upon exposure to air!

Coaxial Electrospinning of PA 66 and NG−RP (NG−RP@PA 66). Solutions of PA 66 with concentrations of 15, 17.5, or 20 wt % were obtained by dissolving the polymer in an appropriate volume of formic acid and dichloromethane (6:4 w/w) with the aid of stirring at 40 °C for 24 h. A suspension of NG−RP (20 mg mL^{-1}) was obtained by dispersing NG−RP (100 mg) in acetic acid (5.0 mL) with the aid of ultrasonication. Nanofibers were prepared using a horizontal

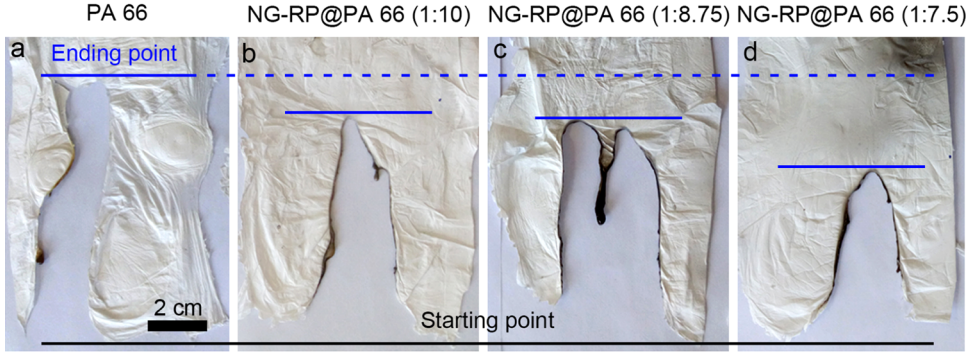

Figure 6. Photographs taken of fabrics composed of the indicated nanofibers after vertical flame testing: (a) neat PA 66; (b) NG−RP@PA 66 (1:10); (c) NG−RP@PA 66 (1:8.75); (d) NG−RP@PA 66 (1:7.5).

DOI: 10.1021/acsomega.7b00397
ACS Omega 2017, 2, 2665−2671

coaxial electrospinning apparatus. A solution of PA 66 and the suspension of NG−RP were separately fed into a syringe pump (Beijing Slgo Medical Technology Co., Ltd.) that was connected to a coaxial spinneret (inner needle: 21-gauge; outer needle: 15-gauge). The spinneret was connected to a high direct current voltage power supply (Tianjin Dongwen High Voltage Power Supply Co., Ltd.), and a voltage of 30 kV was applied between the coaxial spinneret, which was positively biased, and a steel plate that was covered with Al foil. The distance between the coaxial spinneret and the nanofiber collector was measured to be 8 cm. The feeding rates of the solution of PA 66 and the suspension of NG−RP were set to be 0.5 and 2 mL h^{-1}, respectively. The resulting nanofibers were dried in a vacuum oven set at 45 °C for 24 h. All experiments were carried out at room temperature (20−30 °C) with a relative humidity of 40−50%. The nanofibers were prepared by electrospinning solutions of PA 66 in concentrations of 15, 17.5, or 20 wt % and denoted as NG−RP@PA 66 (1:7.5), NG−RP@PA 66 (1:8.75), and NG−RP@PA 66 (1:10), respectively; the ratios in parentheses refer to the weight ratios of NG−RP:PA 66 in the nanofiber feedstocks.

Electrospinning of Neat PA 66 Nanofibers. Neat PA 66 nanofibers were prepared by electrospinning the aforementioned PA 66 solutions using a single 15-gauge spinneret. All of the other parameters were the same as those used to prepare the NG−RP@PA 66 nanofibers described above.

General Characterization Techniques. SEM and EDS elemental mapping were performed using a Hitachi S-4800 microscope. TEM of the NG−RP composites was performed with a JEOL JEM-2100F microscope at 200 kV. TEM of the nanofibers was performed with a JEOL HT7700 microscope at 100 kV. XRD patterns were obtained with a Bruker D8 Focus diffractometer using an incident wavelength of 0.154 nm (Cu Kα radiation) and a Lynx-Eye detector. XPS was performed with a PHI Quantera scanning X-ray microprobe equipped with a monochromated Al Kα radiation source (1486.7 eV). Raman spectra were collected on a Renishaw inVia-Reflex confocal Raman microscope at an excitation wavelength of 532 nm. TGA was performed with a TGA Q50 system at a scanning rate of 10 °C min^{-1}. Mechanical properties were measured using a universal testing machine (Instron-5966; Instron Co. Ltd.) at a crosshead rate of 3 mm min^{-1} on specimens with dimensions of 0.8 cm × 6.0 cm × 50 μm; samples were tested in triplicate and the average values were reported. Vertical flame tests were performed using a CZF-3 type instrument (Jiangning Analysis Instrument Company, China); each sample was tested five times. MCC (MCC-2; Govmark Ltd., McHenry, IL) was performed over the temperature range of 75−750 °C at a heating rate of 1 °C s^{-1}.

■ ASSOCIATED CONTENT

Supporting Information

The Supporting Information is available free of charge on the ACS Publications website at DOI: 10.1021/acsomega.7b00397.

Additional morphology, composition, and thermal data recorded for the NG−RP nanoplatelets as well as the neat PA 66 and NG−RP@PA 66 nanofibers (PDF)

■ AUTHOR INFORMATION

Corresponding Author

*E-mail: jianxingeng@mail.ipc.ac.cn. Tel: +86-10-82543416.

ORCID

Sheng Zhang: 0000-0001-7131-6246

Christopher W. Bielawski: 0000-0002-0520-1982

Jianxin Geng: 0000-0003-0428-4621

Author Contributions

#L. Xiao and L. Xu equally contributed to this work. L. Xu started the ball milling of graphite in the presence of red phosphorus and L. Xiao completed all the laboratory experiments.

Notes

The authors declare no competing financial interest.

■ ACKNOWLEDGMENTS

This work was supported by the "Hundred Talents Program" of the Chinese Academy of Sciences and by the National Natural Science Foundation of China (21274158, 91333114), and CAS President's International Fellowship for Visiting Scientists (2013T1G0019). CWB is grateful to the Institute for Basic Science (Grant IBS-R019-D1) and the BK21 Plus Program as funded by the Ministry of Education and the National Research Foundation of Korea for their support.

■ REFERENCES

(1) McCann, J. T.; Li, D.; Xia, Y. N. Electrospinning of Nanofibers with Core-Sheath, Hollow, or Porous Structures. *J. Mater. Chem.* **2005**, *15*, 735−738.

(2) Wu, J.; Wang, N.; Zhao, Y.; Jiang, L. Electrospinning of Multilevel Structured Functional Micro-/Nanofibers and Their Applications. *J. Mater. Chem. A* **2013**, *1*, 7290−7305.

(3) Ouyang, S.; Wang, T.; Yu, Y.; Yang, B.; Yao, J.; Wang, S. From Trans to Cis Conformation: Further Understanding the Surface Properties of Poly(M-Phenylene Isophthalamide). *ACS Omega* **2017**, *2*, 290−298.

(4) Greiner, A.; Wendorff, J. H. Electrospinning: A Fascinating Method for the Preparation of Ultrathin Fibres. *Angew. Chem., Int. Ed.* **2007**, *46*, 5670−5703.

(5) Li, X.; Yu, X.; Cheng, C.; Deng, L.; Wang, M.; Wang, X. Electrospun Superhydrophobic Organic/Inorganic Composite Nanofibrous Membranes for Membrane Distillation. *ACS Appl. Mater. Interfaces* **2015**, *7*, 21919−21930.

(6) Joseph, J.; Nair, S. V.; Menon, D. Integrating Substrate Less Electrospinning with Textile Technology for Creating Biodegradable Three-Dimensional Structures. *Nano Lett.* **2015**, *15*, 5420−5426.

(7) Jin, L.; Wu, D.; Kuddannaya, S.; Zhang, Y.; Wang, Z. Fabrication, Characterization, and Biocompatibility of Polymer Cored Reduced Graphene Oxide Nanofibers. *ACS Appl. Mater. Interfaces* **2016**, *8*, 5170−5177.

(8) Zhang, H.; Qin, X.; Wu, J.; He, Y.-B.; Du, H.; Li, B.; Kang, F. Electrospun Core-Shell Silicon/Carbon Fibers with an Internal Honeycomb-Like Conductive Carbon Framework as an Anode for Lithium Ion Batteries. *J. Mater. Chem. A* **2015**, *3*, 7112−7120.

(9) Li, Y.-C.; Mannen, S.; Morgan, A. B.; Chang, S.; Yang, Y.-H.; Condon, B.; Grunlan, J. C. Intumescent All-Polymer Multilayer Nanocoating Capable of Extinguishing Flame on Fabric. *Adv. Mater.* **2011**, *23*, 3926−3931.

(10) Moon, S.; Ku, B.-C.; Emrick, T.; Coughlin, B. E.; Farris, R. J. Flame Resistant Electrospun Polymer Nanofibers from Deoxybenzoin-Based Polymers. *J. Appl. Polym. Sci.* **2009**, *111*, 301−307.

(11) Chen, S.; Li, X.; Li, Y.; Sun, J. Intumescent Flame-Retardant and Self-Healing Superhydrophobic Coatings on Cotton Fabric. *ACS Nano* **2015**, *9*, 4070−4076.

(12) Mayer-Gall, T.; Knittel, D.; Gutmann, J. S.; Opwis, K. Permanent Flame Retardant Finishing of Textiles by Allyl-Functionalized Polyphosphazenes. *ACS Appl. Mater. Interfaces* **2015**, *7*, 9349−9363.

DOI: 10.1021/acsomega.7b00397
ACS Omega 2017, 2, 2665−2671

(13) Maji, K.; Haldar, D. POSS-Appended Diphenylalanine: Self-Cleaning, Pollution-Protective, and Fire-Retardant Hybrid Molecular Material. *ACS Omega* **2017**, *2*, 1938−1946.
(14) Yarin, A. L.; Zussman, E.; Wendorff, J. H.; Greiner, A. Material Encapsulation and Transport in Core-Shell Micro/Nanofibers, Polymer and Carbon Nanotubes and Micro/Nanochannels. *J. Mater. Chem.* **2007**, *17*, 2585−2599.
(15) Qu, H.; Wei, S.; Guo, Z. Coaxial Electrospun Nanostructures and Their Applications. *J. Mater. Chem. A* **2013**, *1*, 11513−11528.
(16) Kim, M.-J.; Jean, I.-Y.; Seo, J.-M.; Dai, L.; Baek, J.-B. Graphene Phosphonic Acid as an Efficient Flame Retardant. *ACS Nano* **2014**, *8*, 2820−2825.
(17) Some, S.; Shackery, I.; Kim, S. J.; Jun, S. C. Phosphorus-Doped Graphene Oxide Layer as a Highly Efficient Flame Retardant. *Chem. − Eur. J.* **2015**, *21*, 15480−15485.
(18) Higginbotham, A. L.; Lomeda, J. R.; Morgan, A. B.; Tour, J. M. Graphite Oxide Flame-Retardant Polymer Nanocomposites. *ACS Appl. Mater. Interfaces* **2009**, *1*, 2256−2261.
(19) Nine, M. J.; Tran, D. N. H.; Tung, T. T.; Kabiri, S.; Losic, D. Graphene-Borate as an Efficient Fire Retardant for Cellulosic Materials with Multiple and Synergetic Modes of Action. *ACS Appl. Mater. Interfaces* **2017**, *9*, 10160−10168.
(20) Xing, W.; Yang, W.; Yang, W.; Hu, Q.; Si, J.; Lu, H.; Yang, B.; Song, L.; Hu, Y.; Yuen, R. K. K. Functionalized Carbon Nanotubes with Phosphorus- and Nitrogen-Containing Agents: Effective Reinforcer for Thermal, Mechanical, and Flame-Retardant Properties of Polystyrene Nanocomposites. *ACS Appl. Mater. Interfaces* **2016**, *8*, 26266−26274.
(21) Gao, Y.; Zhang, Y.; Williams, G. R.; O'Hare, D.; Wang, Q. Layered Double Hydroxide-Oxidized Carbon Nanotube Hybrids as Highly Efficient Flame Retardant Nanofillers for Polypropylene. *Sci. Rep.* **2016**, *6*, No. 35502.
(22) Shi, Y.; Long, Z.; Yu, B.; Zhou, K.; Gui, Z.; Yuen, R. K. K.; Hu, Y. Tunable Thermal, Flame Retardant and Toxic Effluent Suppression Properties of Polystyrene Based on Alternating Graphitic Carbon Nitride and Multi-Walled Carbon Nanotubes. *J. Mater. Chem. A* **2015**, *3*, 17064−17073.
(23) Xu, L.; Xiao, L.; Jia, P.; Goossens, K.; Liu, P.; Li, H.; Cheng, C.; Huang, Y.; Bielawski, C.; Geng, J. A Lightweight and Ultrastrong Polymer Foam with Unusually Superior Flame Retardancy. *ACS Appl. Mater. Interfaces*, **2017**, Requested for Revision.
(24) Shen, L.; Phang, I. Y.; Chen, L.; Liu, T. X.; Zeng, K. Y. Nanoindentation and Morphological Studies on Nylon 66 Nanocomposites. I. Effect of Clay Loading. *Polymer* **2004**, *45*, 3341−3349.
(25) Dasari, A.; Yu, Z.-Z.; Yang, M.; Zhang, Q.-X.; Xie, X.-L.; Mai, Y.-W. Micro- and Nano-Scale Deformation Behavior of Nylon 66-Based Binary and Ternary Nanocomposites. *Compos. Sci. Technol.* **2006**, *66*, 3097−3114.
(26) Pan, L.; Zhu, X.-D.; Sung, K.-N.; Liu, Y.-T.; Xie, X.-M.; Ye, X.-Y. Molecular Level Distribution of Black Phosphorus Quantum Dots on Nitrogen Doped Graphene Nanosheets for Superior Lithium Storage. *Nano Energy* **2016**, *30*, 347−354.
(27) Luo, X.; Wang, X.; Bao, S.; Liu, X.; Zhang, W.; Fang, T. Adsorption of Phosphate in Water Using One-Step Synthesized Zirconium-Loaded Reduced Graphene Oxide. *Sci. Rep.* **2016**, *6*, No. 39108.
(28) Xu, J.; Shui, J.; Wang, J.; Wang, M.; Liu, H.-K.; Dou, S. X.; Jeon, I.-Y.; Seo, J.-M.; Baek, J.-B.; Dai, L. Sulfur-Graphene Nanostructured Cathodes Via Ball-Milling for High-Performance Lithium-Sulfur Batteries. *ACS Nano* **2014**, *8*, 10920−10930.
(29) Hu, C.; Xue, J.; Dong, L.; Jiang, Y.; Wang, X.; Qu, L.; Dai, L. Scalable Preparation of Multifunctional Fire-Retardant Ultralight Graphene Foams. *ACS Nano* **2016**, *10*, 1325−1332.
(30) Wang, X.; Quintero Romero, M.; Zhang, X.-Q.; Wang, R.; Wang, D.-Y. Intumescent Multilayer Hybrid Coating for Flame Retardant Cotton Fabrics Based on Layer-by-Layer Assembly and Sol-Gel Process. *RSC Adv.* **2015**, *5*, 10647−10655.
(31) Li, S.; Deng, L.; Xu, C.; Wu, Q.; Wang, Z. Making a Supertough Flame-Retardant Polylactide Composite through Reactive Blending with Ethylene-Acrylic Ester-Glycidyl Methacrylate Terpolymer and Addition of Aluminum Hypophosphite. *ACS Omega* **2017**, *2*, 1886−1895.
(32) Chen, P.; Zhang, F.; Li, S.; Cheng, Y. Smoke Suppression Properties of Epoxy Crosslinked Structure and Intumescent Fire Retardant in Epoxy-Based Intumescent Fire-Retardant Coating. *J. Appl. Polym. Sci.* **2016**, *133*, 8782−8787.
(33) Wang, H.; Yang, C.; Liu, R.; Gong, K.; Hao, Q.; Wang, X.; Wu, J.; Zhang, G.; Hu, Y.; Jiang, J. Build a Rigid−Flexible Graphene/Silicone Interface by Embedding SiO_2 for Adhesive Application. *ACS Omega* **2017**, *2*, 1063−1073.
(34) Yu, B.; Shi, Y.; Yuan, B.; Qiu, S.; Xing, W.; Hu, W.; Song, L.; Lo, S.; Hu, Y. Enhanced Thermal and Flame Retardant Properties of Flame-Retardant-Wrapped Graphene/Epoxy Resin Nanocomposites. *J. Mater. Chem. A* **2015**, *3*, 8034−8044.
(35) Nagendra, B.; Rosely, C. V. S.; Leuteritz, A.; Reuter, U.; Gowd, E. B. Polypropylene/Layered Double Hydroxide Nanocomposites: Influence of LDH Intralayer Metal Constituents on the Properties of Polypropylene. *ACS Omega* **2017**, *2*, 20−31.

DOI: 10.1021/acsomega.7b00397
ACS Omega 2017, 2, 2665−2671